

See discussions, stats, and author profiles for this publication at: <https://www.researchgate.net/publication/231645424>

Scanning Electron Microscopy for in Situ Monitoring of Semiconductor–Liquid Interfacial Processes: Electron Assisted Reduction of Ag Ions from Aqueous Solution on the Surface of Ti...

ARTICLE *in* THE JOURNAL OF PHYSICAL CHEMISTRY C · AUGUST 2010

Impact Factor: 4.77 · DOI: 10.1021/jp1044546

CITATIONS

10

READS

27

2 AUTHORS, INCLUDING:



Andrei Kolmakov

National Institute of Standards and Techn...

132 PUBLICATIONS 4,824 CITATIONS

SEE PROFILE

Scanning Electron Microscopy for *in Situ* Monitoring of Semiconductor–Liquid Interfacial Processes: Electron Assisted Reduction of Ag Ions from Aqueous Solution on the Surface of TiO₂ Rutile Nanowire[†]

Natalia Kolmakova and Andrei Kolmakov*

Physics Department, Southern Illinois University at Carbondale, Illinois 62901

Received: May 16, 2010; Revised Manuscript Received: August 17, 2010

The combination of scanning electron microscopy and environmental cell equipped with electron transparent but yet gas/liquid impenetrable membrane was used for *in situ*, real time monitoring of chemical processes taking place at the surfaces of individual fully hydrated metal oxide nanostructures at nanoscopic scale. Similar to the photoreduction process, it was observed that secondary electrons generated in TiO₂ nanowire by the primary electron beam lead to electron mediated Ag deposition from AgNO₃ solution. The formation and growth of Ag nanoparticles, nanowires, and dendrimeric structures at the TiO₂–liquid interface was investigated. The demonstrated approach has immense potential for real time imaging and rapid, *in vivo* compositional analysis of the interfacial chemical processes relevant to (photo)catalysis, batteries, fuel cells, and environmental remediation.

1. Introduction

The high vacuum requirements imposed when using either conventional scanning or transmission electron microscopy (TEM) present a major limitation when attempting to analyze at the nanoscale the physical and chemical processes taking place in liquids and dense gas media. As a consequence, there has been a persistent trend, mainly in the field of (photo)catalysis,^{1–10} water electrolysis, and decontamination,¹¹ to overcome this so-called “pressure gap” in order to have spectroscopic and microscopy access to the processes taking place under ambient pressure and in liquids.¹² Although attempts to conduct electron microscopy under ambient conditions were undertaken at very early stages of electron microscopy (see reviews 13 and 14 and references therein), tremendous progress along these lines has been achieved more recently as a result of the development of the environmental scanning electron microscope (ESEM) and differentially pumped or sealed environmental cells (E-cells) for TEM.^{15–18}

The latest advancements in large scale fabrication of ultrathin and robust organic and inorganic gas impenetrable membrane materials resulted in the implementation of inexpensive commercial E-cells^{19,20} for the examination of fully hydrated samples in a conventional SEM^{21,22} under conditions which can not be achieved with ESEM. This methodology has a great potential for nanotechnology and materials science to probe *in situ* with nanoscopic resolution the interfacial processes taking place inside the electrochemical, fuel and (photo)catalytic cells and biomedical systems.

In this paper we demonstrate the capabilities of the method to image the electron (hole) mediated processes on the surface of the single crystal TiO₂ rutile nanowire immersed in AgNO₃ solution. The latter system is a well studied prototype for photochemical reduction of the metal ions dissolved in water and therefore is an excellent system to test the proposed approach.

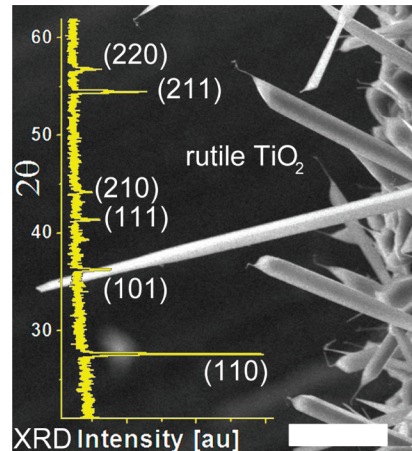


Figure 1. SEM image of the rutile TiO₂ nanostructures grown via combination of carbothermal reduction of titania precursor and thermal oxidation of Ti wire for 2 h at 800–900 °C in 200 Torr Ar with traces of air. The left panel shows the XRD spectrum taken from the nanowire deposit. The scale bar is 7 μ m.

2. Experimental Section

To grow single crystal rutile titania nanowires, the source mixture composed of TiO₂ and graphite powders (1:1 by volume) was heated at 1100 °C in an Ar carrier gas flow (30 sccm, 200 Torr) for 2 h. Pure Ti wire (0.25 mm dia, 99.99%, Alfa Aesar) was placed at 700–800 °C, and titania nanostructures grew on their surfaces. This combination of carbon-assisted (carbothermal)²³ reduction of titania and slow thermal oxidation of Ti wire yields TiO₂ nanowires and whiskers 10²–10³ nm in diameter and 10–30 μ m in length (Figure 1). The XRD taken from the layer of nanowires collected from the surface of Ti wire indicated that TiO₂ nanowires and whiskers possess rutile structure (Figure 1 (left graph)).

The principle of SEM imaging in liquids^{24–27} is depicted in Figure 2. In this study the commercial Quantomix QX-102 cells, initially designed for imaging primarily biological samples (Figure 2a), was used. The interior of the E-cell is isolated from

[†] Part of the “D. Wayne Goodman Festschrift”.

* Corresponding author. E-mail: akolmakov@physics.siu.edu.

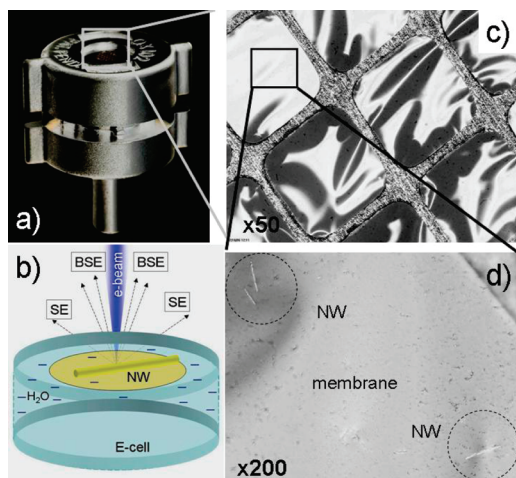


Figure 2. Design and operational principle of the SE microscopy in liquids; (a) the general view of the Quantomix QX-102 cell used in this study; (b) the schematics of the interior of the cell with fully hydrated nanowire (NW) placed in the proximity to the inner side of the membrane; (c and d) the optical images of the top membrane of the cell at two different magnifications $\times 50$ and $\times 200$ correspondingly. The areas containing TiO_2 nanowires are marked with dashed circles.

the vacuum by a thin (150–200 nm), polyimide membrane which is nearly transparent for the 10–30 kV electron beam.²¹ The electron beam penetrates through the membrane, and as a result of interaction with nano-object behind the membrane, the secondary (SE) and backscattered electrons (BSE) are created (Figure 2b). Since predominantly BS electrons from the object are capable of penetrating back through the membrane and leave the E-cell, this channel was used for SEM imaging. The membrane is supported on a reinforcing metal mesh to withstand the pressure difference of 1 bar; thus, the interior of the cell can be filled with gas or liquid up to atmospheric pressure (Figure 2c). In our tests, an aqueous suspension of TiO_2 nanowires (dd H_2O , deionized, and distilled Millipore Milli-Q, purity checked by conductivity $<0.2 \mu\text{S cm}^{-1}$) was deposited onto the inner side of the membrane of the capsule (Figure 2d). After the water completely evaporated, mapping of the location of dry nano(meso) structures deposited on the back surface of the membrane was performed using an optical microscope (Nikon L150). The latter procedure facilitates the prompt location of the nanostructures during SEM examination, thereby minimizing exposure of the nanowires to the electron beam. For ionic solutions, three different concentrations of AgNO_3 (99.9% Alfa Aesar), 10^{-2} , 10^{-4} , and 10^{-5} M in water, were used in the experiments. Two SEM instruments, a conventional SEM (Hitachi S-570) and an environmental SEM (Hitachi S-2460N), were used in the study; the latter SEM was equipped with a Noran 443A energy dispersive spectroscopy (EDS) detector that was used for *in situ* compositional analysis of the hydrated nanostructures. Most of the images in this communication were produced in the conventional SEM, whereas the environmental SEM was used mainly to conduct elemental analyses.

To study of electron beam induced processes in liquid–solid interface comparatively, we used a rutile single crystal TiO_2 nanowire in two different model environments: (i) pure deionized water and (ii) aqueous solutions of silver nitrate at different concentrations. Monte Carlo (MC) simulations of the electron trajectories for polyimide membrane– TiO_2 –water system was performed using Casino v2.42 software.²⁸

3. Results and Discussion

The gray scale coding in the Figure 3 depicts MC simulated absorbed energy profiles along (i) the entire electron interaction volume in water Figure 3a and (ii) when 1 μm thick TiO_2 slab is placed at different distances of 0, 4, and 12 μm (Figure 3b–d, respectively) from the 150 nm polyimide membrane. Due to low atomic number Z of water, the calculated electron range for 30 keV electrons is over 20 μm in liquid water^{21,29} (see Figure 3a). When the sample with larger Z (TiO_2) is located in the proximity of the membrane, the electron range reduces drastically and the appreciable part (ca. 50%) of the electron beam energy is dissipated in the nanostructure (see yellow contour line in the Figure 3b). While low energy SE emitted from the nanostructure becomes attenuated by the membrane (and interfacial water layer(s)), sufficiently more energetic BS electrons from the immersed sample (and from the surrounding liquid) primarily define the signal at the BSE detector. The difference of the back scattered coefficient of media h_M and the sample h_S under the membrane provides the contrast $C_{MS} = (h_S - h_M)/h_S$ in the SEM image. In our case the calculated h_M and h_S were 0.057 and 0.098, respectively, what defined the best simulated imaging conditions with $C_{MS} \sim 0.4$. As it was shown in ref 21, the intimate contact of the sample with the back side of the membrane defines also the best spatial resolution which is comparable to the size of the electron beam. With an increase in the distance between the immersed object to the membrane, h_M and h_S merge following the trend of an increased role of the media in the partitioning of the absorbed energy (see Figure 3b–d). This factor, along with deterioration of the electron beam diameter with the sampling distance in the media defines the limitation of the method which therefore is applicable to the objects located not deeper than approximately 1 μm from the membrane.

The optimal imaging and analysis parameters for SEM depend sensitively on the particular sample and microscope setup. Below are estimations which help to understand the major contributors in the observed phenomena. Assuming an average value for the primary electron beam current to be in the order of 1 nA one can estimate that $I_B \sim 10^{10} \text{ s}^{-1}$ electrons are injected in to the E-cell. MC simulations of the electron trajectories and energy losses in the E-cell for the case depicted in the Figure 3b indicate that (i) only a very small fraction ($\sim 10^{-4}$ – 10^{-5}) of primary electrons with $E_B = 30 \text{ kV}$ will remain inside 1 μm thick TiO_2 whisker (see the Supporting Information) and (ii) the energy fraction of the primary e-beam α as large as 50% is released inside the whisker due to inelastic collisions of primary electrons. As a result of these electron-induced interband transitions in TiO_2 , a large number of electron–hole (e–h) pairs are produced inside the interaction volume in addition to the emitted SE and BS electrons. The generation rate G of the electron–hole pairs in the interaction volume of nanostructure ($V \sim 10^{-12} \text{ cm}^3$) is much larger than the primary electron beam rate I_B and can be evaluated as $G = \alpha(E_B/3E_g)I_B \sim 10^{13} \text{ s}^{-1}$ (here $3E_g$ is an e–h formation threshold and E_g is a band gap $\sim 3.2 \text{ eV}$ for rutile titania). In the macroscopic titania samples and grains, the majority of the generated e–h pairs recombine within the recombination time $\tau \sim 10^{-8} \text{ s}$.³⁰ The latter defines the steady state amount of e–h pairs inside the interaction volume: $n \sim G\tau \sim 10^5$ (this corresponds to ca. 10^{17} cm^{-3}). Since the estimated electron (hole) diffusion length $L = (\tau D)^{1/2} \sim 10^2 \text{ nm}$ is comparable to the radius of the nanostructure r , the significant fraction of the electrons (holes) generated inside the nanowire is capable of reaching the surface of the nanostructure and therefore participates noticeably in surface redox processes.

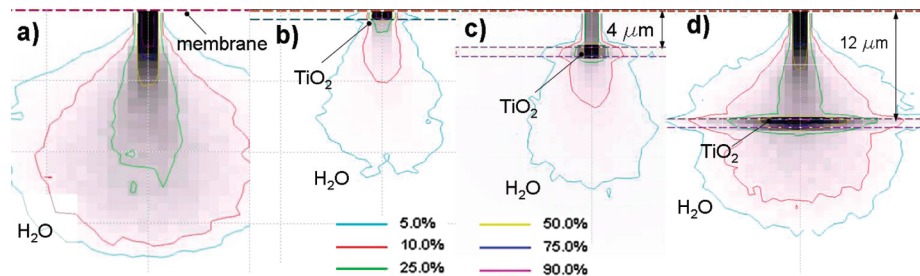


Figure 3. The simulated absorbed energy profiles in (a) pure liquid water and (b–d) when TiO_2 one micrometer thick sample placed correspondingly at 0, 4, and 12 μm below 150 nm polyimide membrane (accelerating voltage 30 kV, number of electron trajectories simulated = 10^4). The contour energy lines and the associated numbers define the percent of energy dissipated beyond the contoured volume.

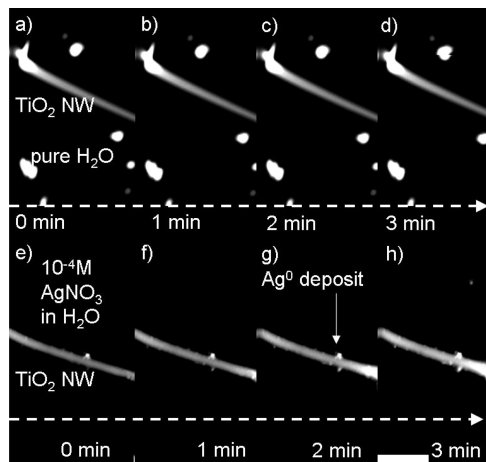


Figure 4. (a–d) Consecutive images of an individual TiO_2 nanowire submerged in ddH_2O and (e–h) 10^{-4} M AgNO_3 in QX-102 wet cell (1 min apart). Instrument used: Hitachi S-570 with BSE detector. Operating conditions: acceleration voltage 30 kV, working distance 11 mm. Scale bar: 2 μm . The irregularly shaped white particles are from debris material attached to membrane.

In our case, the fraction of electrons/holes capable of reaching the surface is even larger due to the high crystallinity of the whisker and the surface band bending of TiO_2 which facilitates the separation of e–h pairs. Therefore, the quantum efficiency and the rate of the redox reaction are defined by the delivery rate of the e-beam generated carriers in the nanowire toward the surface and the rate of the reactants from the solution to the nanostructure surface.

Figure 4 depicts two sets of consecutive images of the TiO_2 nanowires immersed in (i) pure water (Figure 4a–d) and (ii) dilute ionic solution (10^{-4} M AgNO_3 ; Figure 4e–h). As can be seen, no changes occur in morphology and shape of the nanostructure as a result of ca. 240 s of exposure to a 30 keV electron beam in pure water. On the other hand, the presence of Ag cations in the liquid changes the nanostructure surface morphology radically, and the surface of the TiO_2 nanostructure becomes progressively decorated with the particles which have higher brightness in the SEM image compared to TiO_2 support (Figure 4e–h). The latter is characteristic for nucleation and growth of the deposit with larger Z. The comparative local EDS (Figure 5) taken in situ on the liquid ionic solution (area B, Figure 5) and on the decorated TiO_2 nanowire (area A, Figure 5) indicates that the deposit material is pure silver. The small traces of Cr, Fe, and Ni observable in area B compose the common EDS background of the QX-102 cell. There are at least two mechanisms potentially responsible for the metal deposition from the solution on the surface of the titania whisker.

(i) Electron assisted Ag deposition is due to reduction of the Ag ions from the solution at the surface of the titania

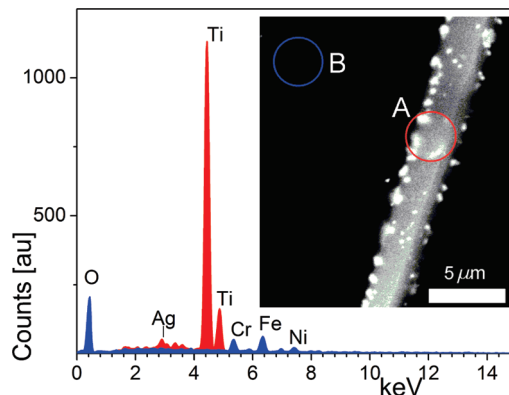


Figure 5. Local EDS taken from the liquid ionic solution (blue, area B) and from the decorated TiO_2 nanowire (red, area A) indicating that the deposit material is pure silver. The small traces of Cr, Fe, and Ni observable in area B are known to be the common EDS background of the QX-102 cell.

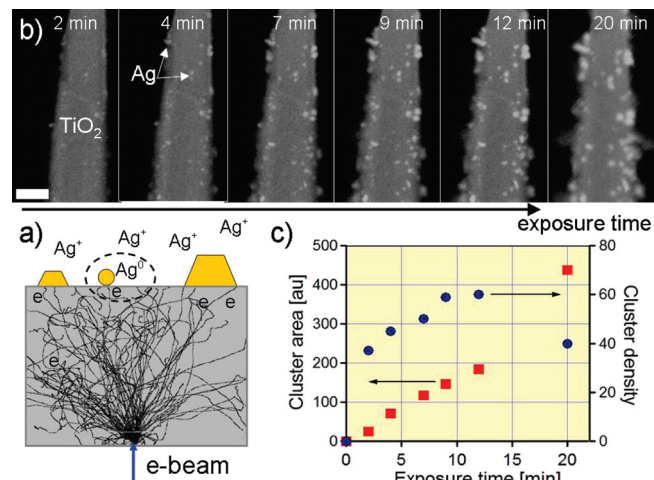
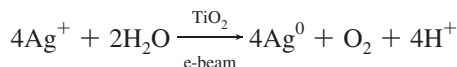


Figure 6. (a) Schematics of the reduction of the Ag cations by the thermalized and secondary electrons at the surface of TiO_2 nanowire; (b) sequential SEM images of a titania whisker immersed in 10^{-4} M aqueous solution of AgNO_3 under continuous scanning with the rate 120 s/frame. Ag nanoparticles nucleation and growth takes place at the surface of titania whisker. Imaging conditions: acceleration voltage, 30 kV; BSE detector; scale bar, 2 μm . (c) The measured total area occupied with nanoparticles (red squares) and particle density (blue dots) as a function of exposure time.

nanostructure induced by electrons which did not recombine with the holes and were able to reach the nanowire–liquid interface (Figure 6a). The stoichiometry of the electron induced reaction taking place at the surface of TiO_2 nanowire submerged in AgNO_3 solution is analogous to well known photoreduction reaction:^{31,32}



where the first 1/2 reaction is a transfer of conduction band electron to the Ag^+ bound to the TiO_2 surface, which finally leads to the growth of Ag^0 clusters with significant quantum yield. As in the case of photocatalysis, the hole transfer to the surface-bound water or hydroxyl groups would serve in this case as the second 1/2 reaction. The rate of this reaction has been previously evaluated by tapping mode AFM based on the size and density of silver particles. It has been demonstrated to be sensitive to titania crystal structure, the energy and flux of photons, and concentration and redox potential of the cation.³³ In our case, it is plausible to assume that the reaction rate of the electron stimulated reduction is limited by the Ag^+ flux from the solution to the nanowire surface. The later can be deduced from the strong dependence of the deposition rate of the concentration of cations in the solution. Similar to pure water, the solution of AgNO_3 at 10^{-5} M concentration did not show a noticeable Ag^0 formation, whereas the immediate heavy coverage of the titania nanowire with Ag was observed at 10^{-2} M concentration. In addition, at 10^{-2} M and higher concentrations the appearance of the high contrast nanoscopic mobile features uniformly distributed over the scanning area can be observed (not shown here). These features can be assigned to beam induced formation of Ag colloids in the solution as a result of the reduction of Ag ions by solvated electrons. It is necessary to note that commonly observed evolution of gaseous products in the form of bubbles at counter electrode or at the nanostructure itself cannot be noticed due to rather slow rate of the electron stimulated reaction. When the electron beam energy is low and recombination kinetics is fast (α and τ are low), the amount of the directly injected primary electrons can be comparable or even prevail the amount of steady state concentration of secondary e-h pairs. Under these conditions the metal deposition proceeds through the mechanism similar to one described below.

(ii) Alternatively, Ag^+ reduction can be simply a result of metal electroplating from the solution on to the TiO_2 whisker via $\text{Ag}^+ + \text{e}^- \rightarrow \text{Ag}^0$ reaction route. The driving force behind this process would be the e-beam induced build up of the potential difference between negatively charged whisker (cathode) and metallized (grounded) E-SEM body (anode). The complete discrimination between the two aforementioned mechanisms requires further studies. However, when the rastering of the e-beam was deactivated, we recorded the predominant Ag depositions localized at those areas which were exposed to the focused beam. The latter observation points toward the dominance of the first mechanism.

Close inspection of SEM micrographs of the TiO_2 whiskers immersed in dilute ionic solution (10^{-4} M AgNO_3 in dd H_2O) reveals the fine details of the nucleation and growth dynamics of the Ag nanostructures. Here we restrict ourselves to only qualitative analysis of nucleation and growth data, due to the experimental trade off between the image resolution and finite scanning rate. For quantitative analysis of the reaction rates and kinetic processes more extensive image set and analysis will be needed in future. The sequential shots of Figure 6b depict few important features of nucleation and growth dynamics: (i) in the early stages the nucleation occurs predominantly at the edges of the titania single crystal nanostructure where the density of the defect sites and/or local electrostatic field are enhanced; (ii) the nucleation density exhibits fast initial growth and saturates approximately at 10 min of constant scanning of the

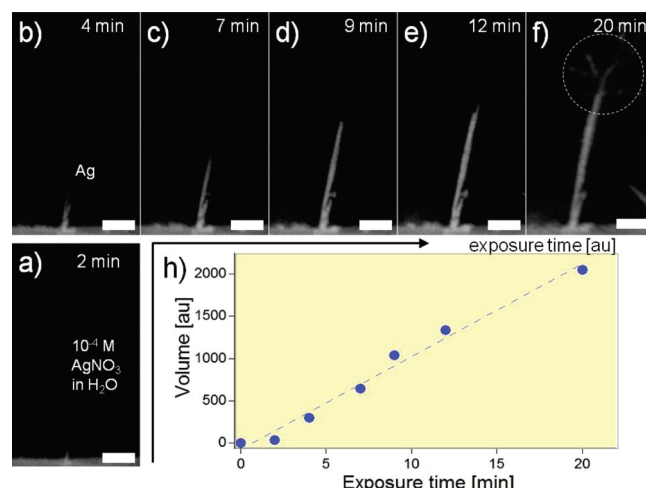


Figure 7. Sequential SEM images taken under continuous scanning of the titania whisker immersed in 10^{-4} M AgNO_3 solution. Quasi 1D growth of Ag nanoparticle is due to preferential reduction of Ag cations at the nanowire apex. The inset reveals nearly linear growth of the nanowire volume with exposure time under electron beam. The circled area in the panel (f) depicts the dendrite-like formation appearing at late stages of the metal deposition. The scale bar corresponds to $1\ \mu\text{m}$.

electron beam (see Figure 6c); (iii) the nanoparticles size increases steadily and at higher exposure the percolation of nanoparticles takes place. The latter is responsible for effective drop of the cluster density at later stages of electron assisted Ag deposition. This characteristic behavior is a manifestation of the diffusion (ion delivery) limited growth of the individual clusters which nucleation density saturates when the diffusion fields of the individual clusters start to overlap at later stages of deposition (see for example ref 34 and references therein).

While most of the Ag deposits accept the morphology of quasi-hemispherical nano- and mesoparticles, a fraction of ca. 1–5% of growing particles possess peculiar shape which implies the existence of the factors complementing the aforementioned diffusion dominated growth mode. The origin of these unusual growth modes requires more detailed studies, but it was noticed that these nanostructures are often observed at sharp corners (or morphological defects) of studied TiO_2 samples (see Figure 2S in the Supporting Information). The sequential shots in Figure 7 depict the evolution of electron beam-induced growth of the elongated whisker. This quasi one-dimensional growth mode points toward the site specific electron assisted reduction of Ag^+ . In particular (i) the preferable growth takes place at the apex of the Ag nanowire; (ii) it proceeds at a nearly linear rate (Figure 7b); (iii) the growth rate is significantly faster in comparison to the growth of nanoparticles; and (iv) the growth instabilities arise at later stages of Ag nanowire growth what results in formation of the fractal-like structures at the nanowire tip (Figure 7). The needle like shape and preferable formation of the elongated Ag nanostructures at the sharp corners of the TiO_2 support imply that the growth of these nanostructures can be mediated by the electrostatic field. The fast growth rate (ca. 500 nm/min) coupled with the significant Debye length in the diluted solutions ($L_D > 100$ nm) indicates that local electrostatic field at the apex of e-beam irradiated Ag nanowire, if exist, extends deep into solution, what promotes the effective capture of ionic species. The latter observation can be used for rational site specific growth of the nanostructures in liquid and dense gas environments.

4. Outlook

In this paper we demonstrated that SEM imaging combined with E-cell technology can be a valuable tool not only for *in vivo* observation of bio samples^{22,35,36} but also for *in situ* monitoring of the interfacial processes relevant to the photo-(electro)catalysis, electrochemistry, water remediation, fuel cell technologies, etc. The great promise of this technique stands on the fact that imaging can be performed at nanoscale using a standard SEM combined with a backscattered electron (BSE) detector to monitor readily the morphological evolution of fully hydrated samples and/or selected areas of the same sample having different atomic number Z. As exemplified above, the visualization of the fine dynamics of the interfacial processes like electron induced reduction of metal ions over the surface of individual nano(meso)objects submerged in liquid phase can be done under ambient conditions (1 atm). Similarly, the morphological changes taking place at the electrodes/membranes of batteries and fuel cells during the electrochemical reactions can be explored at nanoscale in real time with simultaneous EDS chemical characterization. In addition, electron beam-induced reactions and electrostatic fields in liquids along with preselected supports can be used for beam-assisted growth of the nanostructures. Finally, these experiments also pave the way to the development of the analog of electron beam induced deposition (EBID) process in liquids. Coupled with electrochemistry, the latter will have drastically increased selectivity and yield of deposition compared to its vacuum analog. Furthermore, a much greater moiety of chemical and bio species can be used for EBID in liquids. Since the flushing of the gas or liquid media inside the cell can be easily done without braking vacuum inside SEM, sequential deposition/functionalization with nanoscopic resolution of different species can be achieved.

Acknowledgment. The authors thank Prof. John J. Bozzola, Ms. Hilarie Gates, and Dr. Steven Schmitt (SIUC IMAGE Center) for assistance with the experiments. The research was supported by through NSF ECCS-0925837 award.

Supporting Information Available: Additional data, figures, and refs. This material is available free of charge via the Internet at <http://pubs.acs.org>.

References and Notes

- (1) Stoltze, P.; Norskov, J. K. *Phys. Rev. Lett.* **1985**, *55*, 2502.
- (2) Linsebigler, A. L.; Lu, G. Q.; Yates, J. T. *Chem. Rev.* **1995**, *95*, 735.
- (3) Weiss, W.; Schlogl, R. *Top. Catal.* **2000**, *13*, 75.
- (4) Freund, H. J.; Kuhlenbeck, H.; Libuda, J.; Rupprechter, G.; Baumer, M.; Hamann, H. *Top. Catal.* **2001**, *15*, 201.
- (5) Ertl, G. *J. Mol. Catal. A: Chem.* **2002**, *182*, 5.
- (6) Goodman, D. W. *J. Catal.* **2003**, *216*, 213.
- (7) Kolmakov, A.; Goodman, D. W. *Rev. Sci. Instrum.* **2003**, *74*, 2444.
- (8) Ozensoy, E.; Min, B. K.; Santra, A. K.; Goodman, D. W. *J. Phys. Chem. B* **2004**, *108*, 4351.
- (9) Somorjai, G. A.; York, R. L.; Butcher, D.; Park, J. Y. *Phys. Chem. Chem. Phys.* **2007**, *9*, 3500.
- (10) McClure, S. M.; Goodman, D. W. *Chem. Phys. Lett.* **2009**, *469*, 1.
- (11) Herrmann, J. M. *Top. Catal.* **2005**, *34*, 49.
- (12) Brown, G. E.; Henrich, V. E.; Casey, W. H.; Clark, D. L.; Eggleston, C.; Felmy, A.; Goodman, D. W.; Gratzel, M.; Maciel, G.; McCarthy, M. I.; Nealson, K. H.; Sverjensky, D. A.; Toney, M. F.; Zachara, J. M. *Chem. Rev.* **1999**, *99*, 77.
- (13) Boyes, E. D.; Gai, P. L. *Ultramicroscopy* **1997**, *67*, 219.
- (14) Sharma, R.; Weiss, K. *Microsc. Res. Tech.* **1998**, *42*, 270.
- (15) Daulton, T. L.; Little, B. J.; Lowe, K.; Jones-Meehan, J. *Microsc. Microanal.* **2001**, *7*, 470.
- (16) Gai, P. L.; Calvino, J. J. *Annu. Rev. Mater. Res.* **2005**, *35*, 465.
- (17) Sharma, R. *J. Mater. Res.* **2005**, *20*, 1695.
- (18) Radisic, A.; Vereecken, P. M.; Hannon, J. B.; Seaton, P. C.; Ross, F. M. *Nano Lett.* **2006**, *6*, 238.
- (19) Quantomix. WETSEM <http://www.quantomix.com/Hydration.html>.
- (20) SPI. Wet Cell <http://www.2spi.com/catalog/grids/silicon-nitride-wet-cell-kits.php>.
- (21) Thibierge, S.; Zik, O.; Moses, E. *Rev. Sci. Instrum.* **2004**, *75*, 2280.
- (22) Cohen, O.; Beery, R.; Levit, S.; Ilany, J.; Schwartz, I.; Shabtai, M.; Anaby, D.; Cohen, D.; Alfici, R.; Czerniak, A.; Karasik, A. *Thyroid* **2006**, *16*, 997.
- (23) Rao, C. N. R.; Gundiah, G.; Deepak, F. L.; Govindaraja, A.; Cheethamb, A. K. *J. Mater. Chem.* **2004**, *14*, 440–450.
- (24) Satoh, Y.; Mori, S.; Akutsu, H. *Mol. Biol. Cell* **2004**, *15*, 103A.
- (25) Nechushtan, A.; Vainshtein, A.; Horowitz, M.; Sabban, A.; Zik, O. *Mol. Biol. Cell* **2004**, *15*, 104A.
- (26) Golomb, E.; Behar, V.; Vainshtein, A.; Horowitz, M.; Nechushtan, A. *J. Mol. Diagnost.* **2004**, *6*, 438.
- (27) Barshack, I.; Polak-Charcon, S.; Behar, V.; Vainshtein, A.; Zik, O.; Ofek, E.; Hadani, M.; Kopolovic, J.; Nass, D. *Ultrastruct. Pathol.* **2004**, *28*, 255.
- (28) Drouin, D.; Real Couture, A.; Joly, D.; Tastet, X.; Aimez, V.; Gauvin, R. CASINO V2.42—A Fast and Easy-to-use Modeling Tool for Scanning Electron Microscopy and Microanalysis Users, 2007, Scanning Vol. *29*, 92–101.
- (29) Joy, D. C.; Joy, C. S. *J. Microsc.* **2006**, *221*, 84–88.
- (30) Katoh, R.; Murai, M.; Furube, A. *Chem. Phys. Lett.* **2008**, *461* (4–6), 238–241.
- (31) Herrmann, J. M. *Catal. Today* **1999**, *53*, 115.
- (32) Ohtani, B.; Okugawa, Y.; Nishimoto, S.; Kagiya, T. *J. Phys. Chem.* **1987**, *91*, 3550.
- (33) Farneth, W. E.; McLean, R. S.; Bolt, J. D.; Dokou, E.; Barreau, M. A. *Langmuir* **1999**, *15*, 8569.
- (34) Radisic, A.; Ross, F. M.; Seaton, P. C. *J. Phys. Chem. B* **2006**, *110*, 7862.
- (35) Leizerman, I.; Benzon, R.; Anaby, D.; Chajut, A.; Behar, V. *Obesity Res.* **2005**, *13*, A115.
- (36) Thibierge, S.; Nechushtan, A.; Sprinzak, D.; Gileadi, O.; Behar, V.; Zik, O.; Chowers, Y.; Michaeli, S.; Schlessinger, J.; Moses, E. *Proc. Natl. Acad. Sci. U.S.A.* **2004**, *101*, 3346.

JP1044546